

**SIDEBAR 7.2: THE 2017 COASTAL EL NIÑO**—K. TAKAHASHI, V. ALIAGA-NESTARES, G. AVALOS, M. BOUCHON, A. CASTRO, L. CRUZADO, B. DEWITTE, D. GUTIÉRREZ, W. LAVADO-CASIMIRO, J. MARENGO, A. G. MARTÍNEZ, K. MOSQUERA-VÁSQUEZ, AND N. QUISPE

The original concept of El Niño consisted of anomalously high sea surface temperature and heavy rainfall along the arid northern coast of Peru (Carranza 1891; Carrillo 1893). The concept evolved into the El Niño–Southern Oscillation (ENSO; Bjerknes 1969), although the original El Niño and the Southern Oscillation do not necessarily have the same variability (Deser and Wallace 1987), and the strong El Niño episode in early 1925 coincided with cold-to-neutral ENSO conditions (Takahashi and Martínez 2017). To distinguish the near-coastal El Niño from the warm ENSO phase, Peru operationally defines the “coastal El Niño” based on the seasonal Niño 1+2 SST anomaly (ENFEN 2012; L’Heureux et al. 2017). While recent attention has been brought to the concept of ENSO diversity (e.g., “central Pacific” vs “eastern Pacific” events; Capotondi et al. 2015), the coastal El Niño represents another facet of ENSO that requires further study in terms of its mechanisms and predictability.

A strong coastal El Niño developed off the coast of Peru from January to April 2017 (ENFEN 2017; WMO 2017a,b; Takahashi and Martínez 2017; Ramírez and Briones 2017; Garreaud 2018). The changes were dramatic within the cool coastal upwelling region, as daily SST at Puerto Chicama (7.8°S, 79.1°W) increased abruptly from ~17°C by mid-January to a peak of 26.9°C in early February (ENFEN 2017). The mean maximum/minimum air temperature anomalies along the coast ranged between +1.0°C and +2.3°C across the north, central, and southern regions during February–March.

Convective precipitation is activated in the eastern Pacific when SST exceeds a threshold of ~26–27°C (Takahashi and Dewitte 2016; Jauregui and Takahashi 2017). With SST well in excess of 27°C, the southern ITCZ branch (Huaman and Takahashi 2016; Fig. SB7.2a) was very strong between February and March 2017 and extended into the South American continent

(Fig. SB7.2b). The coastal city of Piura (5.2°S, 80.6°W), located at the core of the ITCZ extension, had a February–March precipitation total of 723 mm, which is nearly seven times its normal amount of 106 mm. The largest precipitation anomalies were observed at low and medium elevations on the western slope of the Andes, triggering several floods and mudslides along the Peruvian coast. Mean January–March 2017 river discharge was around 250% of normal in the Santa (9.01°S, 77.76°W), Rímac (11.77°S, 76.46°W), and Cañete (12.77°S, 75.83°W) River basins.

Impacts along the coast were severe. In the northern regions, a total of 50 927 houses were damaged with close to 1.2 million people affected by flooding, and over 76 000 ha of crops were damaged. As is common with El Niño, this event affected marine resources, primarily the anchovies (Ñiquen and Bouchon 2004; Ñiquen et al. 1999), resulting in decreased fat content and early spawning as a reproductive strategy (IMARPE 2017). The estimated growth of the Peruvian gross domestic product in 2017 was 1.3% lower than expected (BCRP 2017).

The coastal El Niño appears to have been initiated by westerly anomalies in the equatorial far-eastern Pacific in January, the largest for that month since 1981, with a northerly component near the coast (Fig. SB7.3a). At upper levels, the Bolivian high (Lenters and Cook 1996) was located west of its normal position, and a subtropical ridge spread from the Northern Hemisphere, resulting in easterly anomalies and divergence favorable for convection over northwestern Peru (Kousky and Kayano 1994; Vuille et al. 2000). The Madden–Julian oscillation (MJO) had its highest amplitudes in the second half of January and was dominated by the MJO phases 1 to 3, which feature westerly anomalies in this region, according to the Real-time Multivariate MJO index (RMM; Wheeler and Hendon 2004; see Section 4c). The northerly component

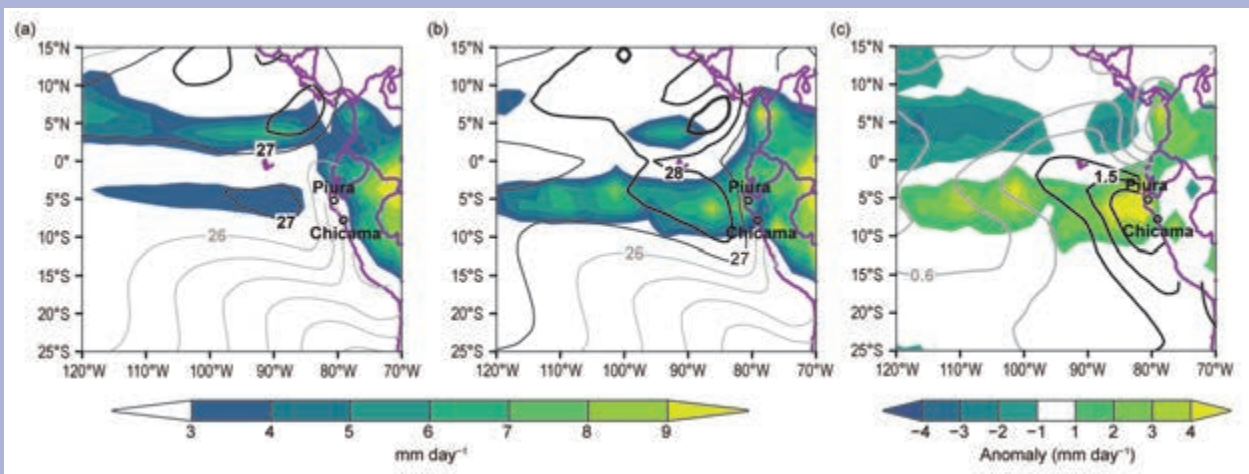


**FIG. SB7.2.** Feb–Mar SST (contours, interval 1°C) and rainfall (shading, mm day<sup>-1</sup>): (a) 1981–2010 climatology, (b) 2017 observations, and (c) 2017 anomalies (contour interval: 0.25°C). (Sources: SST: ERSST v5; rainfall: CMAP.)

was probably associated with the negative mean sea level pressure anomalies in the southeast Pacific (Fig. SB7.3a). The latter could have been associated with Rossby-wave teleconnections from the western Pacific (Garreaud 2018), but the SLP anomalies also extended zonally uniformly across the subtropical South Pacific (Fig. SB7.3a), consistent with the negative phase of Antarctic Oscillation (M 2000a), while the subtropical anomalies closer to the coast of South America were probably partly a response to preexisting positive SST anomalies in that region.

In early February, rainfall in the southern ITCZ became active, and the subsequent growth and maintenance of the event was consistent with the ocean–atmosphere mechanisms proposed for the 1925 coastal El Niño (Takahashi and Martínez 2017), that is, positive feedback between surface warming to the south of the equator, enhanced southern branch of the ITCZ, and reinforced near-equatorial northerly surface wind anomalies (Figs. SB7.3b,c; e.g., Xie and Philander 1994). The strong coastal ocean warming off northern Peru ( $> +2^{\circ}\text{C}$ ) was limited to a shallow layer of about 30 m until the end of February, consistent with local surface forcing (Garreaud 2018). This, jointly with the smaller regional basin scale, explains the much faster timescale of this event (Takahashi and Martínez 2017). The termination of the event in April (Fig. SB7.3d) was also abrupt, as the insolation-driven seasonal sea surface cooling (Takahashi 2005) deactivated the southern branch of the ITCZ, shutting down the feedback mechanism. We should note that toward the end of March, the subsurface warming off northern Peru became deeper (down to 180 m; ENFEN 2017) and persisted until May, probably associated with local ocean–atmospheric Bjerknes feedback (Takahashi and Martínez 2017; Dewitte and Takahashi 2017), although warm ENSO conditions did not materialize (L’Heureux et al. 2017; also see Section 4b), similar to 1925.

The knowledge of the basic mechanism of the 1925 coastal El Niño guided the official Peruvian forecasts in

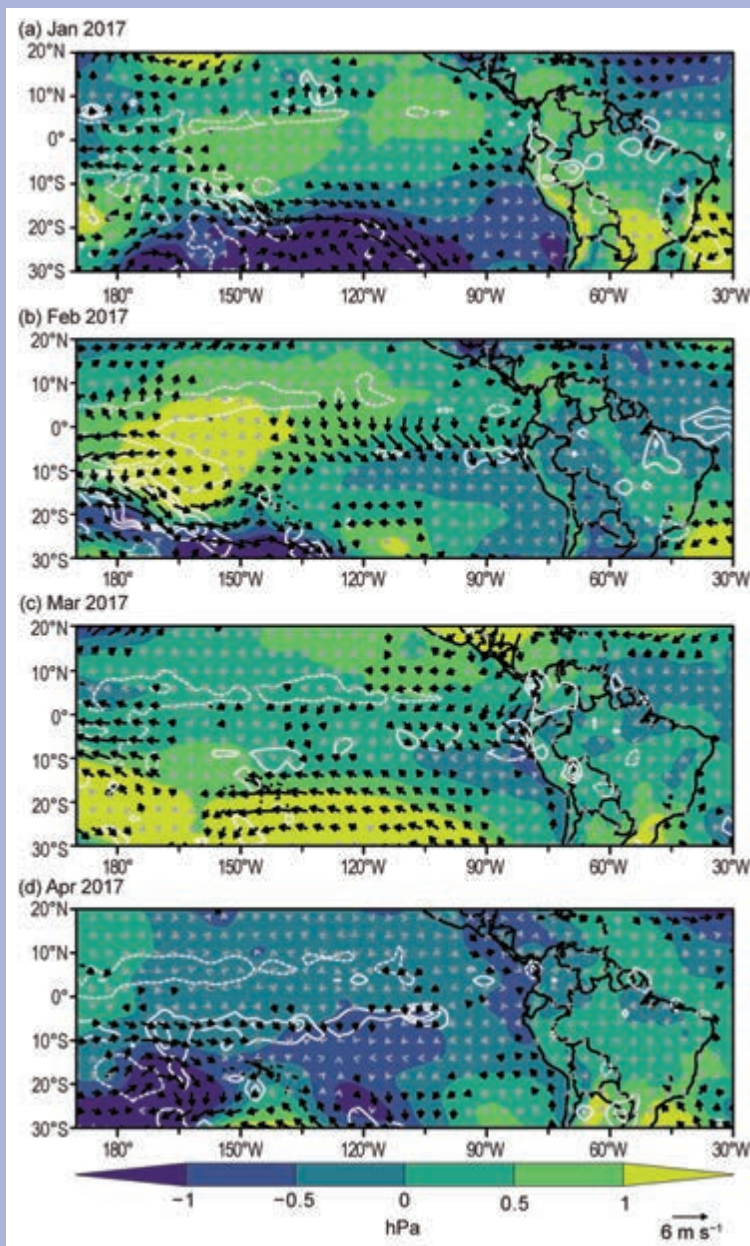


**FIG. SB7.3.** Mean sea level pressure (shading, hPa), 10-m wind (vectors,  $\text{m s}^{-1}$ ;  $>1 \text{ m s}^{-1}$  in black), and precipitation [contours:  $3 \text{ mm day}^{-1}$ , solid (dashed) contours represent positive (negative) anomalies. Zero not shown]. (Sources: MSLP and wind: ERA-interim; precipitation: CMAP.)

2017, but only once the event started in late January, since international climate models provided little indication that such an event would occur (ENFEN 2017). Extending the lead time and accuracy of the prediction of coastal El Niño events is a critical challenge for Peru and requires increased understanding and improved models for this region.